arXiv:1311.5582v1 [cond-mat.dis-nn] 21 Nov 2013

Parallel Tempering Simulation of the three-dimensional Edwards-Anderson Model with Compact Asynchronous Multispin Coding on GPU

Ye Fang[a,b], Sheng Feng[a,c], Ka-Ming Tam[a,c], Zhifeng Yun[a,d], Juana Moreno[a,c], J. Ramanujam[a,b], Mark Jarrell[a,c]

[a]*Center for Computation and Technology, Louisiana State University, Baton Rouge, LA 70803, USA*
[b]*School of Electrical Engineering and Computer Science, Louisiana State University, Baton Rouge, LA 70803, USA*
[c]*Department of Physics and Astronomy, Louisiana State University, Baton Rouge, LA 70803, USA*
[d]*Center for Advanced Computing and Data Systems, University of Houston, Houston, TX 77204, USA*

Abstract

Monte Carlo simulations of the Ising model play an important role in the field of computational statistical physics, and they have revealed many properties of the model over the past few decades. However, the effect of frustration due to random disorder, in particular the possible spin glass phase, remains a crucial but poorly understood problem. One of the obstacles in the Monte Carlo simulation of random frustrated systems is their long relaxation time making an efficient parallel implementation on state-of-the-art computation platforms highly desirable. The Graphics Processing Unit (GPU) is such a platform that provides an opportunity to significantly enhance the computational performance and thus gain new insight into this problem. In this paper, we present optimization and tuning approaches for the CUDA implementation of the spin glass simulation on GPUs. We discuss the integration of various design alternatives, such as GPU kernel construction with minimal communication, memory tiling, and look-up tables. We present a binary data format, Compact Asynchronous Multispin Coding (CAMSC), which provides an additional 28.4% speedup compared with the traditionally used Asynchronous Multispin Coding (AMSC). Our overall design sustains a performance of 33.5 picoseconds per spin flip attempt for simulating the three-dimensional Edwards-Anderson model with parallel tempering, which significantly improves the performance over existing GPU implementations.

Keywords:
Spin Glass, Edwards-Anderson Model, Ising Model, Parallel Tempering, Multispin Coding, GPU, CUDA.

1. Introduction

Stochastic or Monte Carlo (MC) simulation is one of the most important methods in the study of complex interacting systems. However, even with the huge success of Monte Carlo methods, many systems remain very difficult to simulate. The main obstacle very often is the long required simulation time, while the memory demands are quite modest. A prominent example is the Edwards-Anderson (EA) model, where the inherent randomness and frustration lead to very long relaxation times. Although the EA model has been intensively simulated over the past few decades, including implementations using gate-level reconfigurable processors [1] and some dedicated computers designed specifically for solving this model, [2, 3, 4, 5, 6] many aspects are still far from completely understood. Some prominent topics, such as the nature of the spin glass phase below the upper critical dimension, remain highly debated issues. [7, 8, 9, 10, 11, 12, 13, 14, 15, 16, 17, 18]

The Graphics Processing Unit (GPU) provides an opportunity to significantly improve the computational performance of Monte Carlo simulations of classical systems. Massive parallelism and acceleration can be achieved by implementing these algorithms on GPUs. In the past few years some GPU accelerated simple spin models have been proposed, including the two-dimensional Ising model by Hawick et al. [19] and Block et al. [20], and the Ising model in the cubic and network lattices by Preis et al. [21]. Weigel [22, 23] studied the Ising and the Heisenberg models in both two- and three-dimensional lattices. These implementations focus predominately on unfrustrated systems with large lattice sizes. In this study, we mainly focus in the simulation of a random frustrated Ising system in equilibrium. Due to its slow relaxation rate, a large number of Monte Carlo steps are required, at the same time the system sizes that can be simulated are relatively small, in most cases limited to only a few thousands sites. Precisely because of these characteristics, Monte Carlo simulations of random frustrated systems are a good match for the GPU computing architecture.

Our implementation targets cluster computers with NVIDIA Fermi GPUs. Using C/CUDA we control and tune details of the program. We expose the inherent parallelism of the algorithm to the GPU accelerator, including parallel computation on multiple sites, multiple temperature replicas and multiple disorder realizations. The memory requirements are efficiently handled through memory tiling. In addition, the computation is simplified and vectorized using table look-ups and the Compact Asynchronous Multispin Coding (CAMSC). We also substitute all floating point arithmetic with integer or bit string computations while preserve the same precision. Combining various tuning techniques, we achieve an average spin flip time of 33.5 picoseconds. This is the fastest GPU implementation for the random frustrated Ising system on a 16^3 cubic lattice, and is comparable to that obtained with a field programmable gate array (FPGA) hardware [24] for small to intermediate system sizes. We note that a very recent preprint reported a faster speed in a new FPGA system [25].

The paper is organized as follows. In Section 2, we discuss the algorithm. In section 3, we present an outline of the code framework. The implementation and optimization methods are described in Section 4. Section 5 shows the experimental results. Conclusions and future directions are described in Section 6.

2. Theoretical Background

2.1. Spin Glass

The discovery of a plethora of unusual magnetic behaviors in disordered materials initiated the field of glassy systems.[26] Spin glasses are beyond the conventional description of long range magnetic ordering, e.g., ferromagnetic ordering. Some of their features, including their frequency-dependent susceptibilities and the discrepancy between zero-field and field cooling measurements, suggest that spin glasses have very slow dynamics. Notwithstanding most experimental spin glass systems, which exhibit glassy behavior, randomness and frustration seem to share some common properties. In real materials, dilution introduces randomness and directional or distance-dependent couplings, such as dipolar interactions in insulating systems and the Ruderman-Kittel-Kasuya-Yoshida coupling in metallic systems, introduce frustration.

The simplest model that captures the consequences of disorder is an Ising model with quenched randomly disordered couplings. This model was first proposed by Edwards and Anderson. [27] The mean field solution of the EA model for infinite dimensions was first attempted by Sherrington and Kirkpatrick. [28] However, the replica symmetric mean field solution was found to be unstable below the Almeida-Thouless line, [29, 30] a line in the temperature-field plane below which replica symmetry is broken. The difficulty of obtaining a stable solution was solved by Parisi with his replica symmetry breaking ansatz. [31, 32, 33, 34, 35, 36] Although the mean field solution has been proven to provide the exact free energy for the spin glass phase in infinite dimensions, [37, 38] the spin glass physics in finite dimensions, which presumably is more relevant to experiments, is still not fully understood. Indeed, it had long been debated whether a spin glass phase at finite temperatures exists in three dimensions.

The EA model may be deceptively simple. Since it is a classical spin model, one may think that its numerical study can be simply carried out by Monte Carlo methods on conventional hardware. One of the defining signatures of spin glass systems is their long relaxation time. For sufficiently low temperatures, the system becomes very sluggish and equilibration is prohibitively difficult even for modest systems sizes. Moreover, it has been shown that finding the ground state of the three dimensional EA model is an NP-hard problem. [39] Until recently, there has been no consensus on whether there is a finite spin glass critical temperature in the three dimensional EA model.

The breakthrough in the numerical study of spin glass systems came with the introduction of the parallel tempering method. It allowed the study of larger systems at lower temperatures than the simple single spin flip method. [40, 41, 42] Combined with improved schemes for finite size scaling, it is now widely believed that the thermodynamic finite-temperature spin glass phase does exist in the three dimensional EA model [43]. As the upper critical dimension of the model is six [44, 45, 46], a prominent remaining question is the nature of the spin glass phase below the upper critical dimension [47]. In particular, if the spin glass can still be described by the replica symmetry breaking scenario, there should be an Almeida-Thouless line below the upper critical dimension. A possible test of whether the Almeida-Thouless line exists is to determine whether a spin glass phase exists under an external magnetic field. Correlation length scaling analysis seems to suggest the absence of the spin glass phase in cubic lattices when a finite external field is applied.[9] On the other hand, a recent study in four-dimensional lattices suggests that by using a different quantity for the finite size scaling analysis, a spin glass phase can be revealed. [15] Given the relevance of spin glasses and the on-going controversy on the nature of the spin glass phase below the upper critical dimension, it is desirable to implement an efficient parallel tempering Monte Carlo algorithm using graphics processing units to accelerate the simulations. In this work we show that using the multispin coding method, [48] an efficient Monte Carlo algorithm can be implemented on the GPU.

2.2. Edwards-Anderson Model

We consider the EA Model [27] on a simple cubic lattice. Spins on each lattice site have two states $S_i = +1$ or -1. The couplings J_{ij} are between nearest neighbors. In this study, we focus on a distribution of the couplings which is bimodal with a mean value of zero. That is, there are equal numbers of anti-ferromagnetic and ferromagnetic couplings. The effect of the distribution is certainly a non-trivial problem. We choose to focus on the bimodal distribution because it is best suited for multispin coding. In addition, a constant external field, h, is included in our implementation. The Hamiltonian is given by

$$H = -\sum_{i,j} S_i J_{ij} S_j + h \sum_i S_i. \qquad (1)$$

2.3. Single Spin Flip Metropolis Algorithm

We implement the Metropolis algorithm as our sampling method. The spins are visited and tested for flipping according to the probability $P = \exp(-\beta\Delta E)$, where β is the temperature and ΔE is the energy change associated with the proposed spin flip. As the algorithm satisfies detailed balance, the sampling will generate a distribution according to the partition function provided that the simulation is performed long enough. This type of Monte Carlo simulation is called a Markov process, because the evolution of the state only depends on the state at the current step, and not on its history.

2.4. Parallel Tempering

For the simulation of glasses, the local single spin update algorithm is very slow in thermalizing the system. This problem is particularly severe when the temperature is close to the critical temperature for the second order transition. For certain spin glass models where random dilution is sufficiently large, some form of cluster algorithm can improve the rate of thermalization. Unfortunately, there is no efficient cluster methods for general spin glass systems. The possible exceptions are some random diluted systems or systems in low dimension [49, 50, 51]. Various other methods have been proposed in the past to improve the rate of thermalization including the umbrella sampling, the multi-canonical method, and rejection-free methods. It is now widely accepted that the parallel tempering method is one of the most efficient algorithms for improving the thermalization rate of general spin glass systems.

Parallel tempering uses several samples of the system within a range of temperatures (Figure 1). The low temperature sample is more difficult to thermalize due to the larger barriers between low energy configurations [42, 41]. However, as the probability to swap the configuration between the high and the low temperature samples increases, the chance of the system to escape from a local minima in the low temperature sample also increases. The efficiency of such a parallel tempering move can be measured by the time it takes for a sample to perform a round trip along the temperature axis, that is from the lowest to the highest temperature and back to the lowest temperature. This largely depends on the system being simulated. Fine tuning the range of temperatures and the spacing between them is crucial to optimize the performance. Some recent proposals have been tested on the non-disorder Ising model [52, 53, 54]. Models with explicit disorder such as the EA lack an efficient general method. For a practical GPU implementation, one also needs to consider the effect of the number of replicas on the performance.

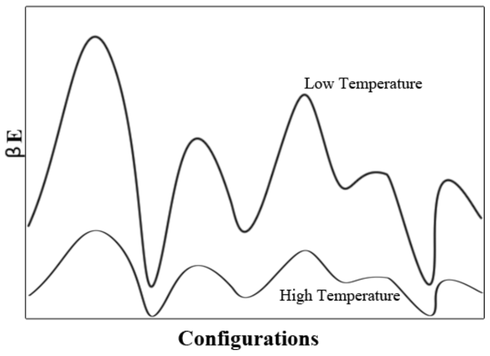

Figure 1: Schematic diagram of the free energy landscape. At high temperatures (small β) the barriers between configurations are reduced allowing the system to search through configurations more efficiently.

3. The Framework

The GPU implementation is discussed in this and the following sections. In our replica exchange spin glass simulation we exploit three levels of parallelism:

1. Several tens of thousands, or more, of independent disorder realizations are required to obtain good statistics.
2. For each disorder realization, usually a few tens of systems at different temperatures are needed to study the physics, such as the possibility of a critical point. We denote these systems as temperature replicas. In the parallel tempering simulation, different temperature replicas communicate with each other only during the parallel tempering swap; these swaps are performed after every few Metropolis single spin sweeps of the lattice.
3. We are mainly interested in systems on bipartite lattices. These are lattices that can be divided in two sub-lattices (A and B) with same sub-lattice spins do not directly coupling with each other. As a result, the update of the A sublattice is independent of the B sublattice.

These three levels of inherent parallelism allows an efficient GPU implementation. In this section we focus on the main structure of the code, which consists of three parts: (i) distributing the spin updates into different GPU threads; (ii) distributing different disorder realizations into different GPU blocks; and (iii) integrating and vectorizing the bit computations of many temperature replicas

3.1. Map Lattice Sites to GPU Threads

The spin lattice is represented by a three dimensional primitive cubic system. To update the sites in the lattice, we follow the common practice of employing a checkerboard decomposition that splits the sites into two sub-lattices shown in blue and red in Figure 2 . Since a blue site is surrounded by red sites and never directly interacts with other blue sites and vice-versa, it is permissible to update each sub-lattice in parallel. We construct two consecutive stages concentrating independently on each of the sub-lattices for parallel computation. The combination of the two stages delivers a lattice sweep of Monte Carlo updates. The lattice is assigned to a GPU thread block, and sites are split across the threads. Details about the lattice site to thread mapping will be discussed in Section 4.2 where we discuss memory optimizations. The total available thread-level parallelism is half of the total lattice sites, and specifically, falls into the range between $8^3/2 = 256$ to $16^3/2 = 2048$ since our simulation targets lattices between 8^3 to 16^3 sites.

3.2. Map Temperatures Replicas to Bits

The parallel tempering technique facilitates the systems to achieve equilibrium. We choose the temperature as the tempering parameter and generate systems with the same couplings but different temperatures, called temperature replicas. The temperature replicas are uncorrelated during the spin-flip process and can therefore be updated in parallel. However, they communicate and swap temperatures (Figure 3) after a few Monte Carlo sweeps. To better utilize the parallelism of multiple temperature replicas and minimize the communication overhead we have developed the Compact Asynchronous Multispin Coding (CAMSC), where spins from different temperature replicas at the same position are encoded into an integer. This leads to sub-word vectorization and a significant reduction of memory transactions. Details of our multispin coding procedure can be found in Section 4.3.3. The number of temperature replicas depends on the system size and the temperature range. In our simulation we used 24 replicas for smaller systems, and 56 temperatures for bigger systems (for example, 10^3 and 12^3).

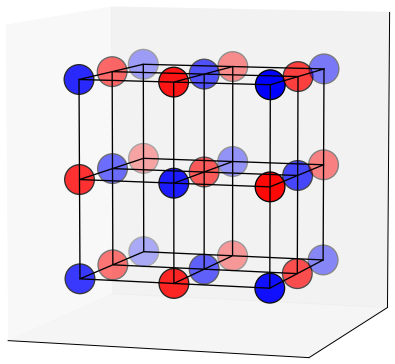
Figure 2: A demonstration of the 3D checkerboard decomposition. The blue and red sites are on different sub-lattices. Since the sites in a sub-lattice never directly interact with each other, it is permissible to update different sites in parallel.

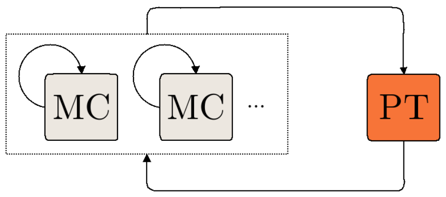

Figure 3: Many temperature replicas can be simulated simultaneously, each using an independent Monte Carlo process. These replicas may be exchanged after a configurable steps of updates. A single GPU thread block is responsible for updating all the Monte Carlo processes and manipulating the parallel tempering exchange.

3.3. *Map Realizations to GPU Blocks*

Spin glass simulations usually require a larger number of disorder realizations (10^4 or more) for reliable disorder averaging. A realization including all temperature replicas has been designated to a thread block. We launch numerous thread blocks across multiple GPUs of multiple hosts until we get the sufficient number of realizations for disorder averaging (Figure 4). To distribute these jobs across multiple nodes, we employ a Pthreads/MPI wrapper for the job distribution.

3.4. *Discussion*

Some parallel processes are sequentialized for better memory locality. For example, although the temperature replicas could be fully parallelized as individual tasks or a lattice may be partitioned across multiple thread blocks, we avoid these forms of parallelism. The remaining parallelism is rich enough (with 10^4 or more thread blocks) to fully occupy the cluster.

To evaluate the performance, we employ a performance metric of average time (in picoseconds) per proposed spin flip for a single GPU card:

$$t = T_{\text{total}}/N_{\text{MCS}}/\left(N_{\text{spins}} \times N_T \times N_{\text{samples}}\right), \qquad (2)$$

where T_{total} is the total wall time of a simulation; N_{MCS} is the number of Monte Carlo sweeps; N_{spins} is the number of spins within a lattice; N_T is the number of temperature replicas; N_{samples} is the total number of disorder realizations on one GPU card. We develop and benchmark the code on a NVIDIA GeForce GTX 580 GPU. Detailed platform configurations can be found in Section 5.

4. Implementation

We discuss implementation details in this section, including the construction of the GPU kernel, memory optimization, and various techniques used to simplify the computation.

4.1. *Kernel Organization Optimization*

Our simulation starts with the Pthreads/MPI job dispatcher that forks many CPU processes across the cluster computer system. Each CPU process is responsible for initiating a lattice realization, which is offloaded to its attached GPU for simulation until the spin variables or thermal averaged results are retrieved from the GPU back to the CPU for analysis.

The GPU workload has three major components (Figure 5):

1. **Metropolis moves**: The Metropolis steps for the single spin update for each temperature replica. This is done by calculating the local energy change and then comparing the acceptance ratio to a uniformly distributed random number.
2. **Parallel tempering moves**: Parallel tempering swaps are performed after a few complete Monte Carlo sweeps of the lattice. This step requires the calculation of total energy for all temperature replicas; we use this to evaluate the acceptance ratio of parallel tempering swaps.
3. **Measurements**: The spin configurations are dumped to the GPU global memory periodically to provide data for the measurements. In practice, we perform one measurement for every few thousands Metropolis sweeps.

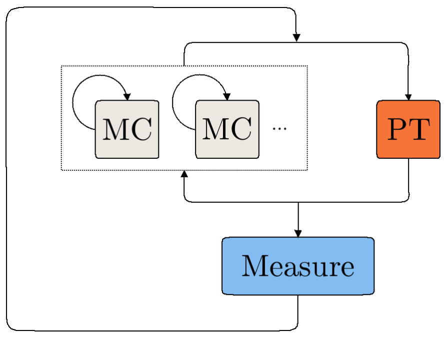

Figure 5: Three major components of the GPU program. One kernel calls Monte Carlo and parallel tempering, implemented as two device functions. Measurement is implemented as a separate GPU kernel.

The measurement code has little overlap with the Monte Carlo and parallel tempering codes, and it is called much less frequently. We implement this part of the code as an separate GPU kernel.

Both Monte Carlo and parallel tempering functions compute spin local energies. Parallel tempering requires additional steps to sum the local energies. Since an efficient implementation of sum (a form of reduction) consumes a considerable amount of shared memory, it may be efficient to separate the parallel tempering as a dedicated GPU function apart from the Monte Carlo. We denote this scheme **MC-PT separated**. Alternatively, the **MC-PT integrated** scheme combines both the Monte Carlo and parallel tempering in a single GPU kernel. Benchmarks (Figure 6) show that the **MC-PT separated** scheme always performs better regardless of the frequency of parallel tempering. However, we find that roughly 10 full Monte Carlo sweeps of the lattice between parallel tempering attempts is a speed/effectiveness sweet point.

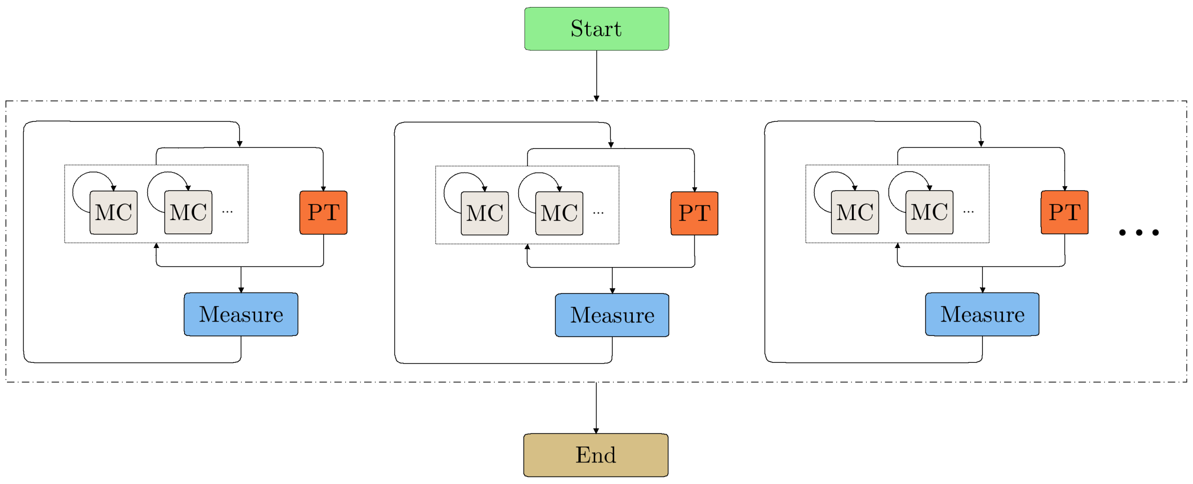

Figure 4: The outline of the simulation application. Disorder realizations are completely independent and can run simultaneously. Each realization contains a unique Monte Carlo parallel tempering process as depicted in Fig. 3, and is assigned to a GPU thread block. This task level parallelism yields sufficient number of thread blocks and can fully occupy a parallel computer system.

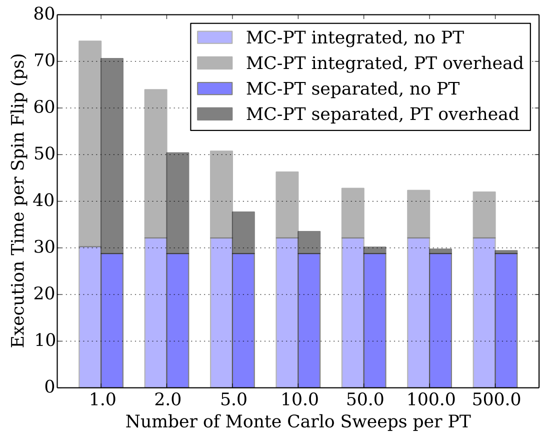

Figure 6: A comparison of the performance of the **MC-PT integrated** and the **MC-PT separated** schemes with different numbers of Monte Carlo sweeps between an attempted parallel tempering swap. The test is conducted with a 16^3 cubic lattice, shared memory probability table of integers, CURAND, and CAMSC.

4.2. *Memory Optimization*

Each spin interacts with its six nearest neighbors (Figure 7) as a seven-point 3D stencil [55, 56] with periodic boundary conditions. Unlike some stencil problems, e.g., the Jacobi finite difference solver for partial differential equations, in which the data for the new time step is completely based on the previous time step, the checkerboard decomposition allows the spin glass simulation to proceed with two consecutive update phases. Only half of the spins are updated in each of the phases. This unconventional stencil, associated with the checkerboard decomposition, leads to a stride-2 memory reference pattern and presents a more challenging memory optimization problem compared to the stride-1 pattern of typical stencils problems.

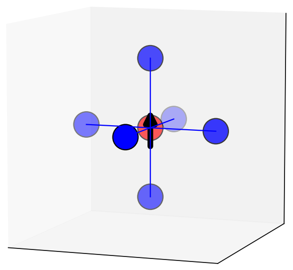

Figure 7: The memory access pattern for a single spin update where in addition to the state of the local spin, we also need the states of its 6 neighbors. Periodic boundary conditions are used.

4.2.1. *Allocation*

We propose three different schemes to address this problem.

1. The **Unified** allocation (Figure 8(a)) stores the checkerboard lattice in its native way as a single piece.
2. The **Separated** allocation (Figure 8(b)) breaks the sub-lattices into two chunks stored separately.
3. The **Shuffled** allocation [57] (Figure 9) mixes and integrates two temperature replicas, so that the memory access pattern is now identical to the conventional stencil. This is done by mixing the two

temperature lattices in such a way that all the A sublattice spins from temperature 1 and the B sublattice spins from temperature 2 are packed together in the memory associated with one lattice. When the spins are being updated on this lattice, they are all independent of each other. They can be considered sequentially and continuously written into memory. Since there is no gap between each memory write, this should theoretically enhance the memory access speed.

The performance comparison on Table 1 suggests that the separated allocation is inferior due to its significantly lower memory performance. This is because of the more complicated control flows in the code. Overall, the unified allocation provides the best memory performance in terms of time spent for each spin and is used in our implementation.

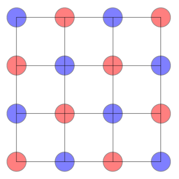
(a) Unified

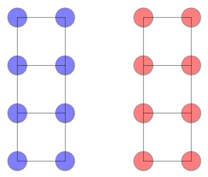
(b) Separated

Figure 8: Unified and separated memory allocation schemes. The unified scheme stores the entire checkerboard lattice together. The separated scheme breaks the memory associated with each sublattice into separate continuous blocks of memory.

	Unified	Separated	Shuffled
Bandwidth(GB/s)	645.1	279.0	832.6
Time per transaction (ps)	49.608	107.756	38.432
Spins per transaction	24	24	16
Time per spin (ps)	2.067	4.345	2.402

Table 1: Performance comparison of the unified/separated/shuffled storage allocation schemes for a 16^3 lattice. The definition of a transaction is a sequence of 7 loads and a store that serve the spin update.

4.2.2. *Tiling for the Multispin Coding Lattice*

The basic idea of multispin coding (MSC) is to present many binaries or short vectors in a longer packed word. For example, Ising spins may be stored with a single bit per spin, with 0 being spin down and 1 being up. In our particular implementation, we also encode the 4 bit string of one site's spin-flip probability table's row index (section 4.3.1) into an integer word. MSC [58**?**] yields a more efficient way of calculating local energies (E) and reduces the memory required for the spin configurations.

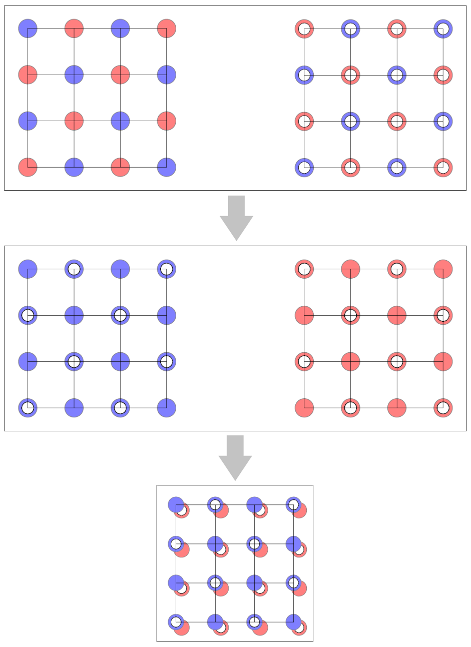

Figure 9: The shuffled allocation mixes and integrates two lattices, shown on the top of the figure. The first transformation is taking the A sublattice on the left (blue dots) and the B sublattice on the right (blue circles) to construct an intermediate lattice (middle left figure of blue color). Another intermediate lattice of red color is constructed similarly. We then integrate these two intermediate lattices together, which occupy different bit positions under the compact multispin coding scheme (Section 4.3.3). By using one integer lattice instead of two, we avoid doubling the memory consumption. Also, the memory access pattern is identical to that of the 7-point 3D Jacobi stencil.

This packing prevents the Arithmetic Logic Unit, which performs integer arithmetic and logical operations, and the memory bandwidth from being under utilized. Also, a memory transaction (7 loads and 1 store) can serve the calculation of multiple spins, which helps improve the relative memory performance.

The usual practice for a single lattice MSC is integrating a line of spins into an integer. We denote this conventional method as Synchronous Multispin Coding (**SMSC**). For the simulation of spin glass models, the temperature replicas provide an alternative approach with a different memory layout. One can pack the spins at a specific site but at different temperature replicas into an integer; we call this the Asynchronous Multispin Coding (**AMSC**). The main idea of these two multispin coding schemes are:

- SMSC: A packed word stores the spins from a single replica, but different sites.
- AMSC: A packed word stores the spins belonging

to different temperature replicas of the same site.

We find the ASMC scheme to be more efficient. Its storage consumption is small enough to fit in the GPU shared memory. Furthermore, AMSC's index system is more straightforward, thereby simplifying optimization. The performance of these different MSC schemes is described below. Here, we briefly discuss how the words associated with either scheme are organized into memory.

Three levels (Figure 10) of the memory hierarchy are employed that reflect the GPU memory architecture of global memory, shared memory and registers:

- **Level 1:** The main data resides in the GPU global memory. Due to the limitation that a 32 bit integer represents at most 32 spins, we may need multiple integer cubes (with an integer cube including one integer per site on the cubic lattice) if there are more than 32 temperature replicas.
- **Level 2:** The shared memory scratchpad holds the working set of an entire integer cube (no larger than $4 \times 16^3 = 16KB$). The data transfer between global and shared memory is quite modest because we do not need to switch to another integer cube until the Monte Carlo and parallel tempering swaps within the temperature replicas contained within the current cube are exhausted.
- **Level 3:** The GPU threads scan the shared memory scratchpad for two consecutive sublattices and load the data into registers. The threads are organized as multiple layers of 2D plates. We observe the optimal thread configurations are two or four layers ($16^2/2 \times 2 = 256$ or $16^2/2 \times 4 = 512$).

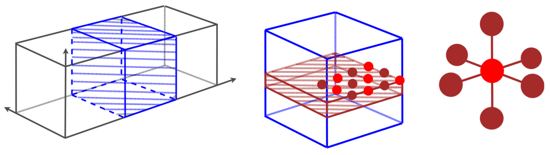
(a) Global Memory (b) Shared Memory (c) Registers

Figure 10: Memory tiling. The global memory may hold several integer cubes (including one integer per lattice site) if there are more than 32 temperature replicas. The shared memory scratchpad holds the working set of an entire integer cube (no larger than $4 \times 16^3 = 16KB$). The registers hold the data needed for local spin updates.

4.3. Optimizing the Computation

We may take advantage of the MSC mapping of the spins onto bits to dramatically reduce the number of floating point operations needed by the Monte Carlo parallel tempering calculations. For example, we may use a bitwise XOR ($\oplus$) as opposed to multiplication to calculate the energy. In the equations below, we denote the variables in the original notation with a superscript ^{o}, and variables without superscripts are used in the transformed notation. The variables S, J, e and E stand for spin, spin coupling, bound energy and local energy respectively.

$$S^o \in \{-1, 1\}, J^o \in \{-1, 1\}$$
$$E_i^o = \sum_j S_i^o \times J_{ij}^o \times S_j^o, E_i^o \in \{-6, -4, -2, 0, 2, 4, 6\}.$$
$$S \in \{0, 1\}, J \in \{0, 1\}$$
$$E_i = \sum_j S_i \oplus J_{ij} \oplus S_j, E_i \in \{0, 1, 2, 3, 4, 5, 6\}.$$

Note that local energy E_i^o, the energy of a spin i in the field of its nearest neighbors, can only take one of seven values as indicated.

The computation is composed of four steps:

1. Energy: Compute the bound energy (e) and the spin's local energy (E).
$$\begin{aligned} e_{ij} &= S_i \oplus J_{ij} \oplus S_j \\ E_i &= \sum_j e_{ij} \end{aligned} \tag{3}$$
2. Probability: Compute the flip probability (P) for the Metropolis Monte Carlo, where the temperature (T) is an input parameters.
$$\begin{aligned} E^o &= 2 \times E - 6 \\ S^o &= 2 \times S - 1 \\ P &= \exp(2 \times (\frac{1}{T} \times E^o + h \times S^o)) \end{aligned} \tag{4}$$
3. Rand: Generate a random number (R).
4. Compare: Compare and update spins.
$$S = (P < R) \oplus S. \tag{5}$$

4.3.1. Probability Look-up Table

Eq. 4 expresses the straightforward yet expensive method to generate the spin flip probabilities. However, since the number of input/output values is finite (i.e., combinations of 7 possible local energies E, 2 spins S, and no more than 32 temperatures T), a better solution is to deploy a pre-calculated look-up table. The table is a two-dimensional matrix (Figure 11), with T as the row index and $(E \times 2 + S)$ as the column index. The column index, as the combination of E and S, requires 4 bits for the address space. The maximum storage consumption of the table is 16 KB, assume that we have 32 rows times 14 columns times 4 bytes per entry (again, assume 32 temperature replicas). When a parallel tempering swap between two replicas at temperatures T_i and T_j is accepted, the two corresponding rows in the table are swapped.

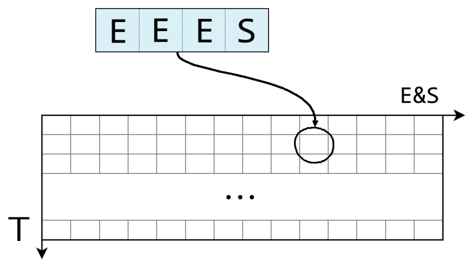

Figure 11: The organization of the probability look-up table.

We evaluate four different ways to calculate the probability in Eq. 4 (Figure 12): (a) using the floating point exponential function from the math library, (b) using a less accurate GPU specialized exponential intrinsic function, (c) using the texture memory to store a table, and (d) a shared memory table. The result shows that an optimal table look-up saves close to half of the total computation time compared to direct computation of the probabilities. In addition, the shared memory table outperforms the texture memory table. This is because GPU threads are simultaneously computing on the same temperature replica, and are therefore accessing the same row of the table. This avoids bank conflicts, so that the high bandwidth and low latency performance potential of the shared memory is fully exploited.

4.3.2. *Random Number Generator*

The simulation requires uniformly distributed random numbers between zero and one. However, due to the fact that pseudo random number generators (RNGs) manipulate integer values internally, directly using integer return values from the RNG provides higher performance and preserves identical precision. As a consequence, we convert the pre-generated probabilities from single precision floating point numbers to 32 bit unsigned integers.

We evaluated three random number generators: (i) NVIDIA CURAND library of XORWOW algorithm [59], (ii) rand123 [60] philox4x32_7 (version 1.06), and

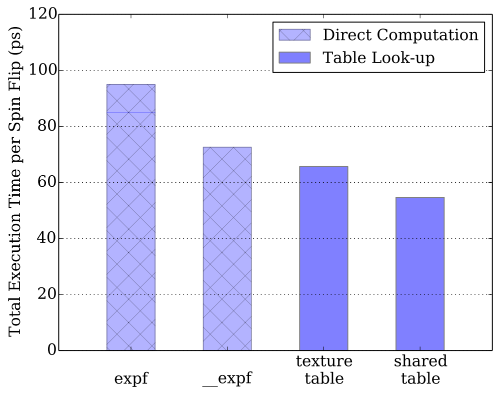

Figure 12: A comparison of the overall time consumed per spin flip using four different methods to compute the exponential probability in Eq. 4 as described in the main text. The experiment is done for a 16^3 lattice, fp32 CURAND and AMSC1. No parallel-tempering is performed.

(iii) our implementation of a multi-threaded 32 bit linear congruential generator (LCG). We decide to adopt CURAND due to its higher performance (Figure 13) and quality [61].

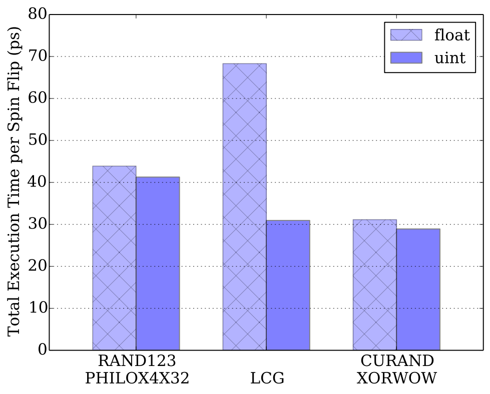

Figure 13: A comparison of the overall time required per spin flip using different random number generators. The experiment used a 16^3 lattice, a shared memory probability table and CAMSC. No parallel-tempering is performed. The loop that consumes random numbers has been unrolled four times to match the four return values of rand123 philox4x32_7.

4.3.3. *Multispin Coding*

We have briefly described the Multispin Coding (MSC). We have developed the Asynchronous Multispin coding (AMSC) as a more efficient alternative to the conventional Synchronous Multispin Coding (SMSC) for calculating the local energies (E), generating the 4

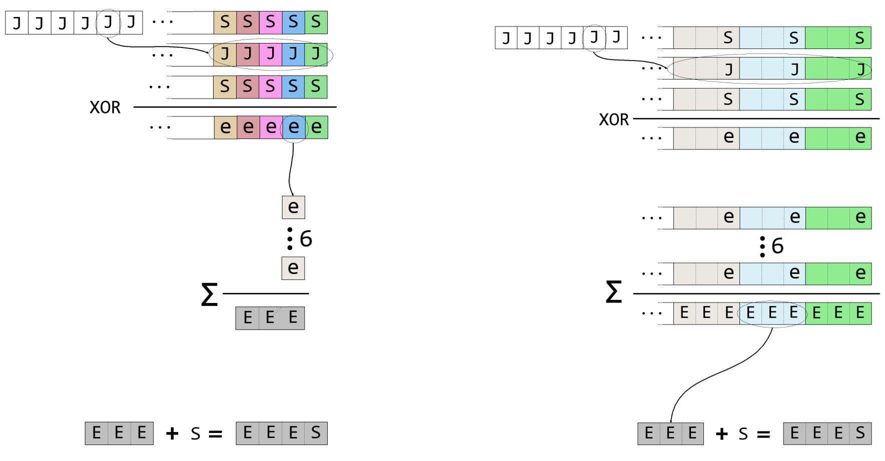

(a) AMSC1 (b) AMSC3

Figure 14: This figure demonstrates the computation of $(E \times 2 + S)$ for the purpose of accessing the probability look up table with the deployment of two variations of Asynchronous Multispin Coding (AMSC). Each line in the figure represents an integer, each box of a line represents a bit, and boxes of the same color represent a segment that hold a variable from one of the temperature replicas. We give the name AMSC1 and AMSC3 for these two AMSC schemes according to their segment width. Unlike the AMSC1, the AMSC3 scheme reserves three bits for each segment, and is a less dense storage format. For the calculation of the local energy, we need two spins (S) and the coupling (J) between them. The J bits and S bits are integrated in the same integer, so that we can fetch both the coupling and the spins using only one memory transaction. The local energy (e) of each bond can be calculated by performing two XOR operations. The total local change of energy (EEE) is the sum of the contributions from all six nearest neighbors. Since EEE requires three bits for storage, the AMSC1 scheme compute each segment sequentially to avoid overflow, while the AMSC3 scheme can compute multiple segments in parallel. After we obtain EEE in three-bit format, we combine it with the spin state (S) by doing string concatenation.

bit string for the column index of the spin-flip probability table (section 4.3.1), and optimizing the memory bandwidth utilization. In our particular GPU implementation, we use four byte unsigned integers, which hold up to 32 bits, as a packed word. Each spin, denoted as 0 or 1, takes only one bit of this packed word. Thus, the calculations in Eq. 3 can be vectorized via bit-wise operations. We integrate the J bits with the S bits in the same integer, so that we can fetch both the coupling and the spins in only one memory transaction. We then multiply the coupling with a bit-mask to match the pattern of S, and calculate the bond energy with bit-wise XOR operation. The next step is to add the six bond energies around a spin to obtain the local energy. To vectorize this process we need to reserve empty bits to avoid overflow, since the local energy takes 3 bits of storage. In this way, each spin, together with the empty bits reserved for calculation, constitute a virtual segment. We derived three variations of AMSC with different segment width of 1, 3 and 4, denoted as AMSC1, AMSC3 and AMSC4 respectively. In AMSC1 and AMSC3, some calculations are sequentialized to avoid overflow. Figures 14 and 15 demonstrate how the the different variations of MSC parallelize the computations in Equations 3, 4 and 5.

Figure 16 illustrates that AMSC3 and AMSC4 are favored over AMSC1 due to improved overall performance. However, we also observe proportionally longer times for the memory transactions. This demonstrates the limitation of the AMSC scheme: there does not exist an optimal segment width that simultaneously provides the highest memory density, and the richest vectorization opportunities in computation.

To overcome the intrinsic limitation of AMSC, we propose a new scheme named Compact Asynchronous Multispin Coding (CAMSC). We dynamically change the segment width to match the data range. Longer width is adopted for larger data to qualify the vectorization of computing multiple segments. For small range data, we use shorter width to avoid blank bits reservations. For example, we allocate 1 bit per segment for S and e, and then expand to 4 bits when calculating E. The segment width expansion is implemented with shift and mask operations. Figure 15(b) demonstrates the procedures of CAMSC and how it differs from traditional AMSCs. Our experiment (Figure 16) shows 28.4% performance improvement when we switch from AMSC3 (46.8 ps/spin) to CAMSC (33.5 ps/spin).

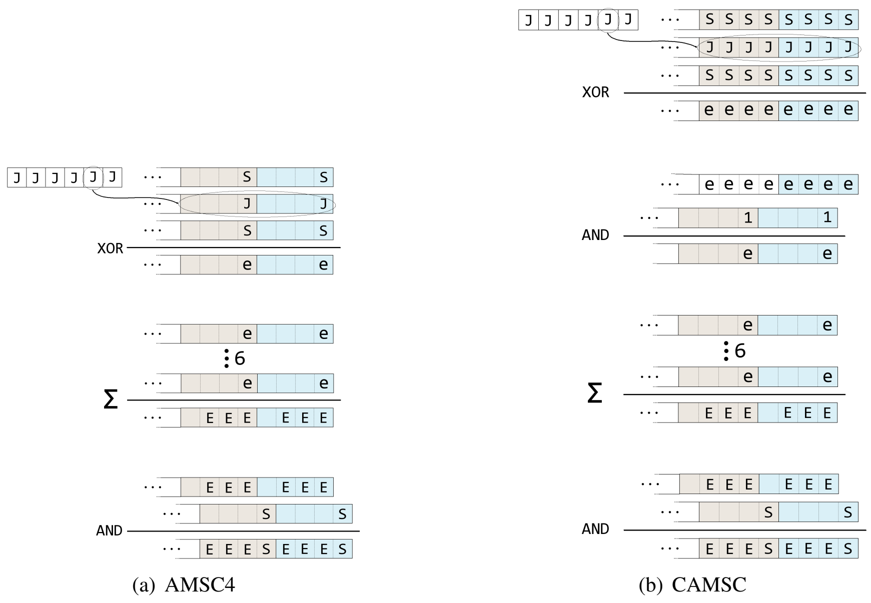

Figure 15: This figure demonstrates how the AMSC4 and CAMSC schemes help exploit bit-level parallelism in computing ($E \times 2 + S$). Similar to that of the AMSC1 and AMSC3 (see the text and the caption of Fig. 14), the XOR operations and summation over six nearest neighbors produces the total local energy (EEE). However, since we reserve four bits for each segment, and is capable of holding one more bit over EEE, the string concatenation of EEE with S can now be vectorized. The difference between CAMSC and AMSC4 is that S and J are stored in a more compact format. With such a design, CAMSC avoids waste of space and provides much better parallelism in computing e.

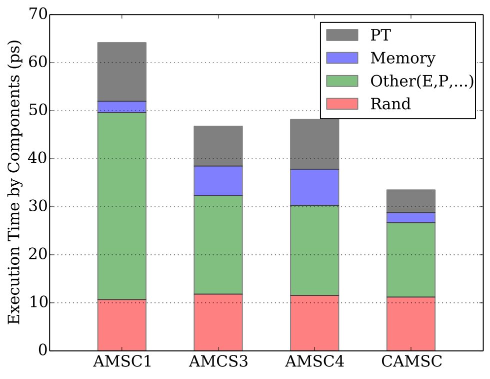

Figure 16: Comparing the performance using different multispin coding schemes. The experiment is done for a 16^3 lattice, a shared memory probability table with integers and CURAND. A parallel-tempering move is performed every 10 Metropolis single spin sweeps.

5. Experimental Results

5.1. The Platform Settings

Our development and performance evaluations are carried out on a workstation with an Intel Core i7 x990 CPU and an NVIDIA GeForce GTX 580 GPU card. The GeForce GTX 580 is equipped with a Fermi architecture GPU of 512 stream processors. We use Linux 2.6.32 x86-64, CUDA toolkit version 4.1 and gcc 4.4.6, and optimization flag -O2. We always configure the GPU on-chip memory as 48KB shared memory plus 16KB L1 cache.

5.2. Performance Evaluation

To evaluate the performance we use the time spent (in picoseconds) per spin flip proposal, abbreviated as ps/spin (See eq. 2).

When we study the equilibrium properties of a spin glass, the system sizes that can be equilibrated within a reasonable time are not very large. Therefore, we used $L = 16$, or $N_{\text{spins}} = 4096$ as the maximum system size. Meanwhile, to achieve efficient parallel tempering moves, we set the number of temperature replicas to $N_T = 24$ or 56, and perform frequent parallel tempering moves (one parallel tempering move after every 5 to 10 Monte Carlo sweeps). The typical number of Monte Carlo steps required to equilibrate such a system is approximately 10^7. Due to the huge sample-to-sample variation, a large number of disorder realizations (10^4 or more) are usually required. However, since there is no correlation among different realizations, we can scatter the jobs to different GPU cards or nodes on a cluster. On each of the cards we only need 16 to 64 realizations to fully utilize all the multiprocessors.

For benchmarking, we simulate 64 disorder realizations of the EA model on a 16^3 lattice with 24 temperature replicas, and propose to swap adjacent temperatures every 10 Monte Carlo sweeps. We are able to complete 10^7 Monte Carlo sweeps in 40 minutes. This wall time consists of the single spin flip Monte Carlo time, the parallel tempering swap time, and the measurement time. Discarding the measurements, the average computational speed is 33.5 ps/spin, for a single GPU device. If we simulate without parallel tempering and serve all temperature replicas with the same random number, we could obtain 17.6 ps/spin. Generating random numbers consumes about one third of the total simulations time, as shown in Figure 16. We believe we are approaching the limit of performance optimization. For reference, our single thread CPU code (using AMSC4 without parallel tempering on a 16^3 cubic lattice) runs at the speed of 14737 ps/spin; this represents a speed up of almost 440 for the GPU code over the CPU code.

Figure 17 compares our implementation with similar existing codes, where not all reference programs target at the random frustrated Ising systems, present the external magnetic field, and feature parallel tempering. Our program is substantially faster than any other GPU implementation [19, 20, 22, 23] for small to intermediate system sizes. We are comparable to the performance achieved by special-purpose FPGA implementations[24].

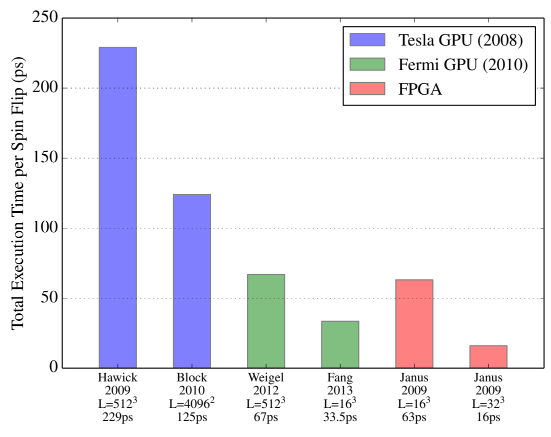

Figure 17: Performance comparison with other heterogeneous Ising model simulation programs. Hawick et al. [19] reports 4360.1 million Monte Carlo hits per second, which equals to 229 ps/spin. Block et al. [20] reports 7977.4 spin flips per microsecond, which equals to 125 ps/spin.

5.3. Simulation Results

We test the code by simulating both the simple ferromagnetic Ising and the EA spin glass models. In Figure 18, our results from the GPU code are found to be consistent with the results from our CPU code for the ferromagnetic Ising model, at various external magnetic fields. We also compare the results with and without parallel tempering as a check to determine whether the parallel tempering swap is performed correctly. We find that the results with and without the parallel tempering swap are consistent with each other. In Figure 19 we plot the correlation length for the ferromagnetic Ising model in three dimensions; here, the crossing point for the correlation length coincides with the known critical temperature for the ferromagnetic ordering. [62] For the EA model we calculate the Binder ratio of the system at zero external magnetic field as shown in Figure 20. The results match reasonably well with the published data. [63] Figure 21 demonstrates the effectiveness of parallel tempering for the EA spin glass. The parallel-tempering simulation reaches equilibrium after 10^5 Monte Carlo sweeps, while without parallel tempering, the system did not reach equilibrium even with 100 times more iterations. This further supports that we have implemented the parallel tempering swapping correctly.

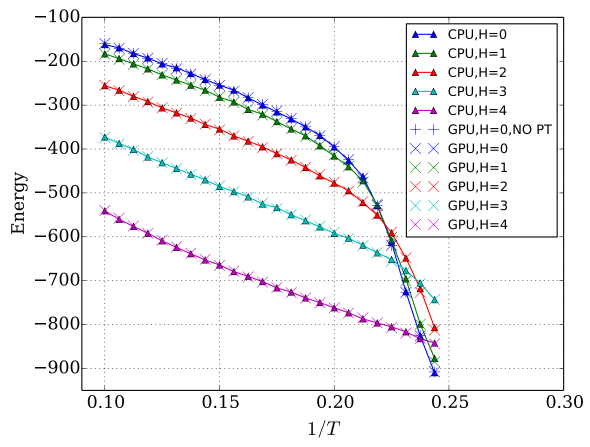

Figure 18: Comparing the total energy of the 16^3 sites Ising model with nearest neighbors coupling $J = -1$, to CPU generated results. At each value of the external field, the GPU results are nearly identical to the CPU results.

6. Conclusion and Future Works

We design and implement a CUDA code for simulating the random frustrated three-dimensional Edwards-Anderson Ising model on GPUs. For small to interme-

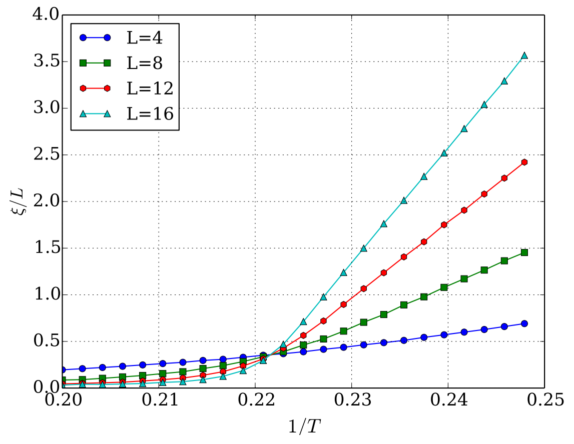

Figure 19: Correlation length vs. inverse temperature for the Ising model. The lines from different system sizes cross close to $1/T = 0.2217$, which is in agreement with the published result for the critical temperature. [62]

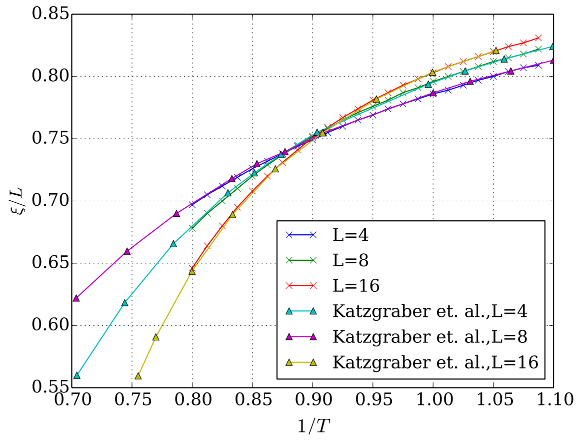

Figure 20: Binder Ratio for the 3D Edwards-Anderson model. The data generated by our GPU code is compared with the data extracted from the paper by Katzgraber *et al.* [63]

diate system sizes, our code runs faster than other GPU implementations, and its speed is close to that of the specially built FPGA computer. We note a very recent preprint has reported an improvement in FPGA system. [25] Our performance tuning strategies include constructing three levels (tasks, threads, bits) of parallel workloads for GPU; optimizing the memory access via a proper data layout and tiling; speeding up the computation by translating time consuming floating point operations to integer point operations and table look-ups; and finally, vectorizing bit computations with our binary format, the Compact Asynchronous Multispin coding.

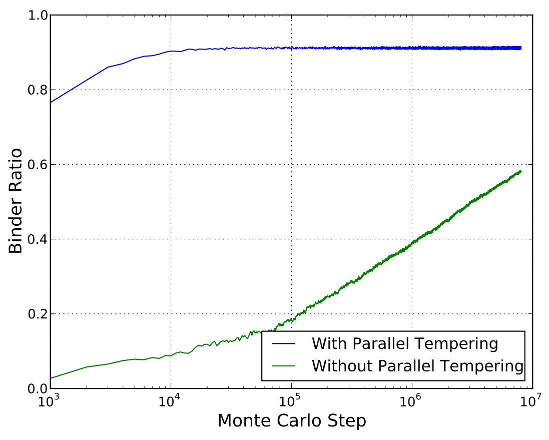

Figure 21: The convergence of the Binder ratio vs. number of Monte Carlo steps for the Edwards-Anderson model in a system with 8^3 sites, with and without parallel tempering for $1/T = 2.0$. Parallel tempering dramatically improves the convergence to equilibrium.

Our program can be extended for other models such as the Potts models and models with different random coupling distributions. The structure of our code may adapt well to upcoming GPUs and future massive parallel accelerators.

Acknowledgments

This work is sponsored by the NSF EPSCoR LA-SiGMA project under award number EPS-1003897. Portions of this research were conducted with high performance computational resources provided by Louisiana State University (http://www.hpc.lsu.edu). Part of this work was done on the Oakley system at the Ohio Supercomputer Center. We thank Helmut Katzgraber and Karen Tomko for useful discussions. We thank the following collaborators: Bhupender Thakur, Ariane Papke, Sean Hall and Cade Thomasson. We thank Samuel Kellar for his careful reading of the manuscript.

References

[1] S. Monaghan, A gate-level reconfigurable Monte Carlo processor, Journal of VLSI signal processing systems for signal, image and video technology 6 (1993) 139.

[2] A. T. Ogielski, I. Morgenstern, Critical behavior of three-dimensional Ising spin-glass model, Phys. Rev. Lett. 54 (1985) 928.

[3] A. T. Ogielski, Dynamics of three-dimensional Ising spin glasses in thermal equilibrium, Phys. Rev. B 32 (1985) 7384.

[4] A. Cruz, J. Pech, A. Tarancón, P. Téllez, C. Ullod, C. Ungil, SUE: A special purpose computer for spin glass models, Computer Physics Communications 133 (2001) 165.

[5] J. H. Condon, A. T. Ogielski, Fast special purpose computer for Monte Carlo simulations in statistical physics, Review of Scientific Instruments 56 (1985) 1691.

[6] M. Taiji, N. Ito, M. Suzuki, Special purpose computer system for Ising models, Review of Scientific Instruments 59 (1988) 2483.

[7] T. Jörg, H. G. Katzgraber, F. Krzakala, Behavior of Ising Spin Glasses in a Magnetic Field, Phys. Rev. Lett. 100 (2008) 197202.

[8] M. A. Moore, The stability of the replica-symmetric state in finite-dimensional spin glasses, Journal of Physics A: Mathematical and General 38 (2005) L783.

[9] A. P. Young, H. G. Katzgraber, Absence of an Almeida-Thouless Line in Three-Dimensional Spin Glasses, Phys. Rev. Lett. 93 (2004) 207203.

[10] T. Temesvári, Almeida-Thouless transition below six dimensions, Phys. Rev. B 78 (2008) 220401.

[11] H. G. Katzgraber, Spin glasses and algorithm benchmarks: A one-dimensional view, Journal of Physics: Conference Series 95 (2008) 012004.

[12] M. Sasaki, K. Hukushima, H. Yoshino, H. Takayama, Absence of spin glass phase in the Edwards–Anderson Ising spin glass in magnetic field, Journal of Magnetism and Magnetic Materials 310 (2007) 1514. Proceedings of the 17th International Conference on Magnetism.

[13] M. Sasaki, K. Hukushima, H. Yoshino, H. Takayama, Scaling Analysis of Domain-Wall Free Energy in the Edwards-Anderson Ising Spin Glass in a Magnetic Field, Phys. Rev. Lett. 99 (2007) 137202.

[14] D. Larson, H. G. Katzgraber, M. A. Moore, A. P. Young, Spin glasses in a field: Three and four dimensions as seen from one space dimension, Phys. Rev. B 87 (2013) 024414.

[15] R. A. Baños, A. Cruz, L. A. Fernandez, J. M. Gil-Narvion, A. Gordillo-Guerrero, M. Guidetti, D. Iguez, A. Maiorano, E. Marinari, V. Martin-Mayor, J. Monforte-Garcia, A. Muoz Sudupe, D. Navarro, G. Parisi, S. Perez-Gaviro, J. J. Ruiz-Lorenzo, S. F. Schifano, B. Seoane, A. Tarancon, P. Tellez, R. Tripiccione, D. Yllanes, Thermodynamic glass transition in a spin glass without time-reversal symmetry, Proceedings of the National Academy of Sciences 109 (2012) 6452.

[16] H. G. Katzgraber, T. Jörg, F. Krzkala, A. K. Hartmann, Ultrametric probe of the spin-glass state in a field, Phys. Rev. B 86 (2012) 184405.

[17] H. G. Katzgraber, D. Larson, A. P. Young, Study of the de Almeida-Thouless Line Using Power-Law Diluted One-Dimensional Ising Spin Glasses, Phys. Rev. Lett. 102 (2009) 177205.

[18] L. Leuzzi, G. Parisi, F. Ricci-Tersenghi, J. J. Ruiz-Lorenzo, Ising Spin-Glass Transition in a Magnetic Field Outside the Limit of Validity of Mean-Field Theory, Phys. Rev. Lett. 103 (2009) 267201.

[19] K. A. Hawick, A. Leist, D. P. Playne, Regular Lattice and Small-World Spin Model Simulations using CUDA and GPUs, Int. J. Parallel Prog. 39 (2011) 183.

[20] B. Block, P. Virnau, T. Preis, Multi-GPU accelerated multi-spin Monte Carlo simulations of the 2D Ising model, Computer Physics Communications 181 (2010) 1549.

[21] T. Preis, P. Virnau, W. Paul, J. J. Schneider, GPU accelerated Monte Carlo simulation of the 2d and 3d ising model, J. Comput. Phys. 228 (2009) 4468.

[22] M. Weigel, Simulating spin models on GPU: A tour, International Journal of Modern Physics C 23 (2012) 1240002.

[23] M. Weigel, Performance potential for simulating spin models on GPU, J. Comput. Phys. 231 (2012) 3064.

[24] Janus Collaboration, M. Baity-Jesi, R. A. Banos, A. Cruz, L. A. Fernandez, J. M. Gil-Narvion, A. Gordillo-Guerrero, M. Guidetti, D. Iniguez, A. Maiorano, F. Mantovani, E. Marinari, V. Martin-Mayor, J. Monforte-Garcia, A. Munoz Sudupe, D. Navarro, G. Parisi, M. Pivanti, S. Perez-Gaviro, F. Ricci-Tersenghi, J. J. Ruiz-Lorenzo, S. F. Schifano, B. Seoane, A. Tarancon, P. Tellez, R. Tripiccione, D. Yllanes, Reconfigurable computing for Monte Carlo simulations: results and prospects of the Janus project, ArXiv e-prints (2012).

[25] Janus Collaboration, M. Baity-Jesi, R. A. Baños, A. Cruz, L. A. Fernandez, J. M. Gil-Narvion, A. Gordillo-Guerrero, D. Iñiguez, A. Maiorano, F. Mantovani, E. Marinari, V. Martin-Mayor, J. Monforte-Garcia, A. Muñoz Sudupe, D. Navarro, G. Parisi, S. Perez-Gaviro, M. Pivanti, F. Ricci-Tersenghi, J. J. Ruiz-Lorenzo, S. F. Schifano, B. Seoane, A. Tarancon, R. Tripiccione, D. Yllanes, Janus II: a new generation application-driven computer for spin-system simulations, ArXiv e-prints (2013).

[26] K. Binder, A. P. Young, Spin glasses: Experimental facts, theoretical concepts, and open questions, Rev. Mod. Phys. 58 (1986) 801.

[27] S. F. Edwards, P. W. Anderson, Theory of spin glasses, Journal of Physics F: Metal Physics 5 (1975) 965.

[28] S. Kirkpatrick, D. Sherrington, Infinite-ranged models of spin-glasses, Phys. Rev. B 17 (1978) 4384.

[29] J. R. L. de Almeida, D. J. Thouless, Stability of the Sherrington-Kirkpatrick solution of a spin glass model, Journal of Physics A: Mathematical and General 11 (1978) 983.

[30] A. J. Bray, M. A. Moore, Replica-symmetry breaking in spin-glass theories, Phys. Rev. Lett. 41 (1978) 1068.

[31] G. Parisi, Infinite number of order parameters for spin-glasses, Phys. Rev. Lett. 43 (1979) 1754.

[32] M. Mézard, G. Parisi, N. Sourlas, G. Toulouse, M. Virasoro, Replica symmetry breaking and the nature of the spin glass phase, J. Phys. France 45 (1984) 843.

[33] G. Parisi, A sequence of approximated solutions to the S-K model for spin glasses, Journal of Physics A: Mathematical and General 13 (1980) L115.

[34] G. Parisi, The order parameter for spin glasses: a function on the interval 0-1, Journal of Physics A: Mathematical and General 13 (1980) 1101.

[35] G. Parisi, Magnetic properties of spin glasses in a new mean field theory, Journal of Physics A: Mathematical and General 13 (1980) 1887.

[36] G. Parisi, The physical Meaning of Replica Symmetry Breaking, eprint arXiv:cond-mat/0205387 (2002).

[37] M. Talagrand, The parisi formula, Annals of Mathematics 163 (2006) 221.

[38] F. Guerra, Broken replica symmetry bounds in the mean field spin glass model, Communications in Mathematical Physics 233 (2003) 1.

[39] F. Barahona, On the computational complexity of Ising spin glass models, Journal of Physics A: Mathematical and General 15 (1982) 3241.

[40] R. H. Swendsen, J.-S. Wang, Replica Monte Carlo simulation of spin-glasses, Phys. Rev. Lett. 57 (1986) 2607.

[41] K. Hukushima, K. Nemoto, Exchange Monte Carlo Method and Application to Spin Glass Simulations, Journal of the Physical Society of Japan 65 (1996) 1604.

[42] E. Marinari, G. Parisi, Simulated Tempering: A New Monte Carlo Scheme, EPL (Europhysics Letters) 19 (1992) 451.

[43] H. G. Ballesteros, A. Cruz, L. A. Fernández, V. Martín-Mayor, J. Pech, J. J. Ruiz-Lorenzo, A. Tarancón, P. Téllez, C. L. Ullod, C. Ungil, Critical behavior of the three-dimensional Ising spin glass, Phys. Rev. B 62 (2000) 14237.

[44] A. B. Harris, T. C. Lubensky, J.-H. Chen, Critical Properties of Spin-Glasses, Phys. Rev. Lett. 36 (1976) 415.

[45] H. Tasaki, On the upper critical dimensions of random spin systems, Journal of Statistical Physics 54 (1989) 163.

[46] J. E. Green, M. A. Moore, A. J. Bray, Upper critical dimension for the de almeida-thouless instability in spin glasses, Journal of Physics C: Solid State Physics 16 (1983) L815.

[47] A. P. Young, H. G. Katzgraber, Absence of an Almeida-Thouless Line in Three-Dimensional Spin Glasses, Phys. Rev. Lett. 93 (2004) 207203.

[48] R. Zorn, H. Herrmann, C. Rebbi, Tests of the multi-spin-coding technique in Monte Carlo simulations of statistical systems, Computer Physics Communications 23 (1981) 337.

[49] J. Houdayer, A cluster monte carlo algorithm for 2-dimensional spin glasses, The European Physical Journal B - Condensed Matter and Complex Systems 22 (2001) 479.

[50] S. Liang, Application of cluster algorithms to spin glasses, Phys. Rev. Lett. 69 (1992) 2145.

[51] T. Jörg, Cluster monte carlo algorithms for diluted spin glasses, Progress of Theoretical Physics Supplement 157 (2005) 349.

[52] E. Bittner, A. Nußbaumer, W. Janke, Make life simple: Unleash the full power of the parallel tempering algorithm, Phys. Rev. Lett. 101 (2008) 130603.

[53] H. G. Katzgraber, S. Trebst, D. A. Huse, M. Troyer, Feedback-optimized parallel tempering monte carlo, Journal of Statistical Mechanics: Theory and Experiment 2006 (2006) P03018.

[54] S. Trebst, M. Troyer, U. H. E. Hansmann, Optimized parallel tempering simulations of proteins, The Journal of Chemical Physics 124 (2006) 174903.

[55] A. Nguyen, N. Satish, J. Chhugani, C. Kim, P. Dubey, 3.5-D Blocking Optimization for Stencil Computations on Modern CPUs and GPUs, in: Proceedings of the 2010 ACM/IEEE International Conference for High Performance Computing, Networking, Storage and Analysis, SC '10, IEEE Computer Society, Washington, DC, USA, 2010, p. 1.

[56] K. Datta, M. Murphy, V. Volkov, S. Williams, J. Carter, L. Oliker, D. Patterson, J. Shalf, K. Yelick, Stencil computation optimization and auto-tuning on state-of-the-art multicore architectures, in: Proceedings of the 2008 ACM/IEEE Conference on Supercomputing, SC '08, IEEE Press, Piscataway, NJ, USA, 2008, p. 4:1.

[57] F. Belletti, M. Cotallo, A. Cruz, L. A. Fernández, A. Gordillo, A. Maiorano, F. Mantovani, E. Marinari, V. Martín-Mayor, A. Muñoz-Sudupe, D. Navarro, S. Pérez-Gaviro, J. J. Ruiz-Lorenzo, S. F. Schifano, D. Sciretti, A. Tarancón, R. Tripiccione, J. L. Velasco, Simulating spin systems on JANUS, an FPGA-based computer, Computer Physics Communications 178 (2008) 208.

[58] M. Creutz, L. Jacobs, C. Rebbi, Experiments with a Gauge-Invariant Ising System, Phys. Rev. Lett. 42 (1979) 1390.

[59] NVIDIA, CURAND guide, Web page, documentation, 2012. `http://docs.nvidia.com/cuda/pdf/CURAND_Library.pdf`.

[60] J. K. Salmon, M. A. Moraes, R. O. Dror, D. E. Shaw, Parallel random numbers: as easy as 1, 2, 3, in: Proceedings of 2011 International Conference for High Performance Computing, Networking, Storage and Analysis, SC '11, ACM, New York, NY, USA, 2011, p. 16:1.

[61] M. Manssen, M. Weigel, A. K. Hartmann, Random number generators for massively parallel simulations on GPU, ArXiv e-prints (2012).

[62] A. M. Ferrenberg, D. P. Landau, Critical behavior of the three-dimensional Ising model: A high-resolution Monte Carlo study, Phys. Rev. B 44 (1991) 5081.

[63] H. G. Katzgraber, M. Körner, A. P. Young, Universality in three-dimensional Ising spin glasses: A Monte Carlo study, Phys. Rev. B 73 (2006) 224432.